Geophysical Journal International

Geophys. J. Int. (2013) **194,** 1849–1865
Advance Access publication 2013 June 14

doi: 10.1093/gji/ggt200

Transient analysis of wave propagation problems by half-plane BEM

M. Panji,[1] M. Kamalian,[2] J. Asgari Marnani[3] and M. K. Jafari[2]

[1] *Department of Civil Engineering, Science and Research Branch, Islamic Azad University,* 1477893855 *Tehran, Iran. E-mail: m.panji@srbiau.ac.ir*
[2] *Geotechnical Engineering Research Center, International Institute of Earthquake Engineering and Seismology, P.O. Box* 3913/19395*, Tehran, Iran*
[3] *Department of Civil Engineering, Technical and Engineering Faculty, Central Tehran Branch, Islamic Azad University,* 1419953491 *Tehran, Iran*

Accepted 2013 May 13. Received 2013 March 17; in original form 2012 September 25

SUMMARY

In this paper, a half-plane time-domain boundary element method (BEM) was presented for analysing the 2-D scalar wave problems in a homogenous isotropic linear elastic medium. Using the existing transient full-plane fundamental solution and asking for the assistance of method of source image to satisfy the stress-free boundary conditions, first, a half-plane time-domain fundamental solution was obtained for displacement and traction fields. Then, the condensed closed-form of half-plane time-convoluted kernels were extracted analytically by applying the time-convolution integral on the determined half-plane fundamental solutions. After implementing the half-plane time-domain BEM in computer codes, its applicability and efficiency were verified and compared with those of the published works by analysing several practical examples. The studies showed that the proposed method had good agreement with the existing solutions. Compared to the full-plane time-domain BEM, half-plane time-domain BEM had more capability and better accuracy as well as much shorter run time. It is obvious that this method can be practically used to analyse the site response in substituting the old-style time-domain BEM formulation as well.

Key words: Site effects; Computational seismology; Wave scattering and diffraction; Wave propagation.

1 INTRODUCTION

In technical literature, different volumetric and boundary methods exist for the analysis of soil dynamics and wave propagation problems, which include finite difference method (FDM), finite element method and boundary element method (BEM). To analyse the infinite and semi-infinite continuous media using finite element or FDMs, the boundaries of the energy absorber should be defined and the considered domain needs to be discretized. In this case, the complexity of problem is doubled and the analysis time is increased. Nevertheless, to reduce 1-D in modelling and satisfy the Sommerfeld's radiation conditions of waves at infinity automatically, boundary element (BE) is a suitable method, especially to analyse various problems with infinite and semi-infinite boundaries (Beskos 1987, 1997).

Although the BEM has been developed in both transformed and time domains, systematic analysis of engineering problems in the time domain has several advantages, from among which combining with other numerical methods and analysing non-linear behaviour, analysing of various problems with time-dependent geometry and obtaining the real valued can be pointed out. The first direct time-domain BE formulation was presented by Friedman & Shaw (1962) for antiplane elastodynamics and Cruse & Rizzo (1968) for in-plane elastodynamics. Cole *et al.* (1978) showed the first general formulation of BE in the time domain for 2-D scalar problems. Niwa *et al.* (1980), Manolis & Beskos (1981) and Manolis (1983) used the time-domain BE for the analysis of 2-D elastodynamics problems and their solutions were compared with responses obtained in the transformed domains. The new form of full-plane time-convoluted kernels and BE formulation was presented by Mansur (1983) for 2-D scalar and elastodynamics problems. His BEM formulation was obtained with regard to Heaviside functions and assuming a triangular shape for time interpolations so that Dominguez (1993) showed a better view for them. Antes (1985) developed the time-domain BE formulation for arbitrary initial conditions and Spyrakos & Antes (1986) was able to take them for dynamic analysis of various problems. However, Spyrakos & Beskos (1986) presented another form of time-domain BEM for plane stress or strain problems but Gallego & Dominguez (1990) showed that their obtained formulation was only a special case of the solutions of previous researchers. Regardless of the Heaviside functions in integration, Israil & Banerjee (1990a,b) were able to show the simpler and more tangible form of full-plane time-convoluted kernels for scalar and elastodynamics problems so that later Kamalian *et al.* (2003) modified their in-plane kernels and implemented that in time-domain BEM algorithm in order to analyse different geotechnical earthquake engineering problems as well.

Finally, works of Yu *et al.* (2000) and Soares & Mansur (2009) for antiplane elastodynamics problems are worth noting in the improvement of time-domain BEM formulation.

Either in the time domain or in the transformed domains, two solving methods are proposed by BEM developers for dynamic analysis of a half-plane medium (Dominguez & Meise 1991). In the first method, researchers use the full-plane BEM formulation; in such a case, the considered model is truncated from a full space and, to satisfy the stress-free conditions on the ground surface, discrete modelling to a distance far away from the interested zone is inevitable. Furthermore, fictitious elements which are called 'enclosing elements' are required to be defined for obtaining the series of matrix elements and avoiding singularity in the integration (Ahmad & Banerjee 1988). Some studies have been done using the above modelling process to analyse the seismic behaviour of various problems and obtain the site response which include works by Sanchez-Sesma & Campillo (1991, 1993) on frequency domain and Kamalian *et al.* (2006, 2007, 2008a,b) on time domain.

In the second method, researchers use the half-plane BEM formulation for modelling their semi-infinite problems. Although in the use of half-plane formulation, implementation is more difficult than the full-plane case, the models are simple and it is not necessary to discrete the ground surface and define the fictitious elements. Therefore, the analysis time is reduced and the accuracy of the modelling is increased. Several authors have obtained the half-plane BEM formulation for in-plane elastodynamics problems in both frequency and time domains (Kontoni *et al.* 1987 in the frequency domain and Richter & Schmid 1999 in the time domain). But, because of numerical difficulties arising from implementation and limitations in modelling different types of problems with various boundary conditions, other researchers have paid little attention to them. On the other hand, not being able to obtain analytical time-convoluted kernels in the time-domain BEM, the approximations is raised and the accuracy of the solutions is reduced.

Because of the simple boundary condition in antiplane elastodynamics formulation, it is possible to present the closed-form half-plane fundamental solutions used in the half-plane BEM. Many studies have been done using half-plane BEM in the frequency domain for seismic analysis of site due to propagating incident *SH* waves (Wong & Jennings 1975; Sanchez-Sesma & Esquivel 1979; Dravinski 1982; Ohtsu & Uesugi 1985; Reinoso *et al.* 1993; Ausilio *et al.* 2008). However, in the time domain, a few studies have been done by half-plane BEM and only works of Rice & Sadd (1984), Hirai (1988) and Belytschko & Chang (1988) can be mentioned. In these studies, the antiplane BEM formulation of pioneer researchers (i.e. Cole *et al.* 1978; Mansur 1983) have been used to obtain half-plane time-convoluted kernels and analyse the ground surface response. The condensed closed-form of half-plane time-convoluted kernels is not clearly shown in their formulation.

A review of the literature showed that obtaining the half-plane time-domain BEM for in-plane problems was extremely complex and unintelligible. On the other hand, more studies that are done by BEM to analyse the scalar wave problems, established on the half-plane formulation, are in the frequency domain. Therefore, in this paper, first, using the transient full-plane fundamental solution of scalar wave equation which was accessible in the literature and asking for the assistance of method of source image, a time-domain half-plane fundamental solution was presented and, then, the simple closed-form of displacement and traction half-plane time-convoluted kernels were extracted analytically by applying the time-convolution integral on them. To demonstrate applicability and efficiency of the expressed half-plane time-domain BEM, several practical examples were analysed and verified by other published solutions. A half-plane under Heaviside-type forcing function as well as a full/truncated semi-circular canyon and an embedded full/truncated circular cavity, due to vertically propagating incident *SH* waves as Ricker wavelets type, was considered in detail. In addition, in order to compare two types of the applied modelling (i.e. in the use of the proposed half-plane time-domain BEM and full-plane time-domain BEM), a separate BEM code established on full-plane case was prepared and, in completely the same conditions, accuracy of the solutions as well as analysis time was evaluated. The main purpose of this paper included demonstrating simple models in the use of the presented half-plane time-domain BEM, especially for site response analysis, dramatically reducing analysis time compared with full-plane case and accurately obtaining the solutions.

2 STATEMENT OF THE PROBLEM

A linearly elastic homogeneous and isotropic half-plane was considered (Fig. 1). The equation of motion for antiplane strain model was as follows:

$$\frac{\partial^2 u(x,y,t)}{\partial x^2}+\frac{\partial^2 u(x,y,t)}{\partial y^2}+b(x,y,t)=\frac{1}{c^2}\frac{\partial^2 u(x,y,t)}{\partial t^2}, \tag{1}$$

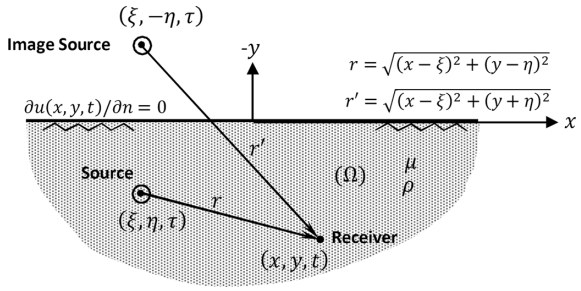

Figure 1. A linearly elastic half-plane due to a concentrated out of plane body force at point (ξ, η) and preceding time τ.

where $u(x, y, t)$ and $b(x, y, t)$ are out of plane displacement and body force at point (x, y) and current time t, respectively, and c is the shear wave velocity given by $\sqrt{\mu/\rho}$, with μ as shear modulus and ρ as mass density. The singular solution of eq. (1), with no regard to any boundary conditions, gave full-plane fundamental solutions. Nevertheless, for a 2-D antiplane semi-infinite media, eq. (1) was solved with the following boundary condition:

$$\mu \frac{\partial u(x, y, t)}{\partial n}\Big|_{y=0} = 0, \tag{2}$$

where n is the normal vector that is perpendicular to the ground surface. Simultaneously, singular solution of eqs (1) and (2) presented the half-plane fundamental solution.

3 SOLUTION METHOD

3.1 Half-plane fundamental solution

To obtain the singular solution of eq. (1) at point (x, y) and time t due to a unit impulsive body force acting point (ξ, η) and preceding time τ, the following can be written (i.e. $b(x, y, t) = \delta(x - \xi)\,\delta(y - \eta)\,\delta(t - \tau)$):

$$\frac{\partial^2 u(x, y, t; \xi, \eta, \tau)}{\partial x^2} + \frac{\partial^2 u(x, y, t; \xi, \eta, \tau)}{\partial y^2} - \frac{1}{c^2}\frac{\partial^2 u(x, y, t; \xi, \eta, \tau)}{\partial t^2} = -\delta(x - \xi)\,\delta(y - \eta)\,\delta(t - \tau), \tag{3}$$

where $\delta(.)$ denotes the Dirac delta function at an assumed point. Application of Fourier transform [denoted by circumflex (ˆ)] to $u(x, y, t; \xi, \eta, \tau)$ with regard to the x-coordinate and Laplace transform (denoted by overbar) with regard to time, that is:

$$u(x, y, t; \xi, \eta, \tau) \Leftrightarrow \hat{u}(k, y, t; \xi, \eta, \tau), \tag{4}$$

$$\hat{u}(k, y, t; \xi, \eta, \tau) \Leftrightarrow \widehat{\bar{u}}(k, y, s; \xi, \eta, \tau). \tag{5}$$

Eq. (3) in the transformed domain will be:

$$\frac{\mathrm{d}^2 \widehat{\bar{u}}(k, y, s; \xi, \eta, \tau)}{\mathrm{d}y^2} - \left(\frac{s^2}{c^2} + k^2\right)\widehat{\bar{u}}(k, y, s; \xi, \eta, \tau) = -\delta(y - \eta)\,\mathrm{e}^{-ik\xi}\mathrm{e}^{-s\tau}. \tag{6}$$

So,

$$\mathcal{F}(\delta(x - \xi)) = \mathrm{e}^{-ik\xi}, \tag{7}$$

$$\mathcal{L}(\delta(t - \tau)) = \mathrm{e}^{-s\tau}H(\tau) = \mathrm{e}^{-s\tau}, \quad \text{if } \tau > 0, \tag{8}$$

in which s is the Laplace transform parameter and k is the Fourier transform parameter (horizontal wavenumber of wave propagation). If a particular solution of eq. (6) is denoted by $\widehat{\bar{u}}^p$, assuming that $k = \alpha s$, it will be:

$$\widehat{\bar{u}}^p(\alpha, y, s; \xi, \eta, \tau) = \frac{1}{2s\beta}\mathrm{e}^{-is\alpha\xi - s\tau - s|y-\eta|\beta}, \tag{9}$$

where

$$\beta(\alpha) = \sqrt{\alpha^2 + \frac{1}{c^2}}, \quad \text{with} \quad \Re(\beta) \geq 0. \tag{10}$$

Eq. (9) is the full-plane fundamental solution of scalar wave equation in the Laplace-wavenumber domain. Without considering the unit impulsive force, eq. (6) will have a homogenous form:

$$\frac{\mathrm{d}^2 \widehat{\bar{u}}(k, y, s)}{\mathrm{d}y^2} - \left(\frac{s^2}{c^2} + k^2\right)\widehat{\bar{u}}(k, y, s) = 0. \tag{11}$$

Assuming that $(s^2/c^2) + k^2 = \phi^2$ and $\widehat{\bar{u}}^h$ denoting the homogenous solution, the answer of above equation is as follows:

$$\widehat{\bar{u}}^h(\alpha, y, s) = A(\alpha, s)\,\mathrm{e}^{-\phi y} + B(\alpha, s)\,\mathrm{e}^{+\phi y}. \tag{12}$$

Eq. (12) may be expressed for the radiating wave going downward:

$$\widehat{\bar{u}}^h(\alpha, y, s) = A(\alpha, s)\,\mathrm{e}^{-\phi y}. \tag{13}$$

The coefficient $A(\alpha, s)$ can be obtained by the boundary condition (2). Therefore, total solution of eq. (1) for a half-plane in the transformed domain will become:

$$\widehat{\bar{u}}(\alpha, y, s; \xi, \eta, \tau) = \frac{1}{2s\beta}\mathrm{e}^{-is\alpha\xi - s\tau - s|y-\eta|\beta} + A(\alpha, s)\,\mathrm{e}^{-\phi y}. \tag{14}$$

Applying the boundary condition (2) to the above equation, the unknown coefficient $A(\alpha, s)$ is obtained as follows:

$$A(\alpha, s) = \frac{1}{2s\beta} \mathrm{e}^{-is\alpha\xi - s\tau - s\eta\beta}, \tag{15}$$

in which $\widehat{\bar{u}}$ denotes the half-plane fundamental solution of 2-D scalar wave equation in Laplace-wavenumber domain. As can be shown, eq. (14) consists of two terms that differ only in a section from each other. This is the method called mirror or image that can be found in several references (Duffy 2001; Haberman 2004). However, the method applied in this study was general and could be used also for different geometries, not just for the half-plane. After applying the Cagniard–De Hoop method (De Hoop 1960) to take the inverse transforms and change the integration path, rearranging the integrals in terms of time parameters, and integrating over the range $[0, +\infty]$ on the hyperbola path, the following equation was obtained for eq. (14) in the space–time domain:

$$u^*(x, y, t; \xi, \eta, \tau) = \frac{1}{2\pi} \left(\frac{H\left((t-\tau) - \frac{r}{c}\right)}{\sqrt{(t-\tau)^2 - \left(\frac{r}{c}\right)^2}} + \frac{H\left((t-\tau) - \frac{r'}{c}\right)}{\sqrt{(t-\tau)^2 - \left(\frac{r'}{c}\right)^2}} \right), \tag{16}$$

where $H(.)$ is the Heaviside function, and r and r' are defined as Fig. 1. $u^*(x, y, t; \xi, \eta, \tau)$ denotes time-domain half-plane displacement fundamental solution at point (x, y) and time t due to a unit antiplane impulsive force at point (ξ, η) and preceding time τ. 2-D full-space transient antiplane elastodynamics fundamental solutions can be found in Morse & Feshbach (1953) and Eringen & Suhubi (1975).

In addition to the half-plane displacement fundamental solution, it is also required to obtain flux or traction fundamental solution for BE formulation. However, taking the differentiation of eq. (16) with regard to the normal can be written as:

$$q^*(x, y, t; \xi, \eta, \tau) = \frac{c}{2\pi} \left(\left[\frac{r H[c(t-\tau) - r]}{\left[\sqrt{c^2(t-\tau)^2 - r^2}\right]^3} \frac{\partial r}{\partial n} \right] + \left[\frac{r' H[c(t-\tau) - r']}{\left[\sqrt{c^2(t-\tau)^2 - r'^2}\right]^3} \frac{\partial r'}{\partial n} \right] \right), \tag{17}$$

where $q^*(x, y, t; \xi, \eta, \tau)$ denotes the time-domain half-plane traction fundamental solution. To carry out the differentiation, $(t-\tau) > r/c$ and $(t-\tau) > r'/c$ were assumed.

3.2 Boundary integral equation (BIE) for external loads

By applying weighted residual integral to eq. (1), eliminating the volumetric integral terms using boundary methods, and ignoring contributions from the initial conditions and body forces, direct BIE in time domain can be obtained as (Brebbia & Dominguez 1989):

$$c(\boldsymbol{\xi})\, u(\boldsymbol{\xi}, t) = \int_\Gamma [u^*(\boldsymbol{x}, t; \boldsymbol{\xi}, \tau) \otimes q(\boldsymbol{x}, \tau) - q^*(\boldsymbol{x}, t; \boldsymbol{\xi}, \tau) \otimes u(\boldsymbol{x}, \tau)]\, \mathrm{d}\Gamma(\boldsymbol{x}), \tag{18}$$

where u^* and q^* are eqs (16) and (17); u and q are displacements and tractions of boundary, respectively. $\Gamma(\boldsymbol{x})$ denotes the boundary of body and $\boldsymbol{x}$ the position vector. $u^* \otimes q$ and $q^* \otimes u$ denote the Riemann-convolution integrals and $c(\boldsymbol{\xi})$ is the geometry coefficient. By defining the time-convolution integral, the above equation can be rewritten as:

$$c(\boldsymbol{\xi})\, u(\boldsymbol{\xi}, t) = \int_\Gamma \left\{ \int_0^t [u^*(\boldsymbol{x}, t; \boldsymbol{\xi}, \tau)\ .\, q(\boldsymbol{x}, \tau) - q^*(\boldsymbol{x}, t; \boldsymbol{\xi}, \tau)\ .\, u(\boldsymbol{x}, \tau)]\, \mathrm{d}\tau \right\} \mathrm{d}\Gamma(\boldsymbol{x}). \tag{19}$$

3.3 BIE for wave scattering

For propagating *SH* waves in a half-plane, total displacement can be decomposed into two parts as follows (Ohtsu & Uesugi 1985; Reinoso *et al.* 1993):

$$u(\boldsymbol{x}, t) = u^{ff}(\boldsymbol{x}, t) + u^{sc.}(\boldsymbol{x}, t), \tag{20}$$

where u^{ff} is the free field displacement of ground surface (without surface irregularities) and $u^{sc.}$ is the contribution of scattered waves. The scattered wavefield is computed by the BEM. In an infinite space, the free field displacement is identical to the incident wavefield $u^{inc.}(\boldsymbol{x}, t)$ because of the radiation condition. Stress-free condition on the ground surface (eq. 2) can be expressed as the following equation for 2-D *SH* wavefield:

$$\frac{\partial u(\boldsymbol{x}, t)}{\partial n} = \frac{\partial u^{ff}(\boldsymbol{x}, t)}{\partial n} + \frac{\partial u^{sc.}(\boldsymbol{x}, t)}{\partial n} = 0. \tag{21}$$

To satisfy eq. (21), a reflected wavefield $u^{ref.}(\boldsymbol{x}, t)$ must be considered with the reverse phase of incident wave so that the free field displacement is obtained with summing incident and reflected wavefield. Considering eq. (20), BIE (eq. 19) must be modified as (Kawase 1988; Hadley *et al.* 1989):

$$c(\boldsymbol{\xi})\, u(\boldsymbol{\xi}, t) = \int_\Gamma \left\{ \int_0^t [u^*(\boldsymbol{x}, t; \boldsymbol{\xi}, \tau)\, .q(\boldsymbol{x}, \tau) - q^*(\boldsymbol{x}, t; \boldsymbol{\xi}, \tau)\, .u(\boldsymbol{x}, \tau)]\, \mathrm{d}\tau \right\} \mathrm{d}\Gamma(\boldsymbol{x}) + u^{ff}(\boldsymbol{\xi}, t)\,. \tag{22}$$

The total displacement is obtained from solving eq. (22). Notably, in order to satisfy the Sommerfeld's radiation condition, while using the models established on full-plane BEM, $u^{inc.}$ substitutes u^{ff} in eq. (22).

3.4 Internal points

Once eq. (22) is solved, it is possible to obtain displacements at any point m in Ω, including the surface $y = 0$ beyond the boundary nodes. To obtain them, the following modified equation is used [$c^m(\boldsymbol{\xi}) = 1$]:

$$u^m(\boldsymbol{\xi}, t) = \int_\Gamma \left\{ \int_0^t \left[u^{*m}(\boldsymbol{x}, t; \boldsymbol{\xi}, \tau) \, . \, q(\boldsymbol{x}, \tau) - q^{*m}(\boldsymbol{x}, t; \boldsymbol{\xi}, \tau) \, . \, u(\boldsymbol{x}, \tau) \right] \mathrm{d}\tau \right\} \mathrm{d}\Gamma(\boldsymbol{x}) + u^{ff.m}(\boldsymbol{\xi}, t), \tag{23}$$

where u^{*m} and q^{*m} are half-plane displacement and traction fundamental solution for each of different internal points, respectively, and $u^{ff.m}$ is free field displacements that should be recalculated.

3.5 Calculation of $c(\boldsymbol{\xi})$

To calculate the geometry coefficient $c(\boldsymbol{\xi})$, the following equation is used (Dominguez 1993):

$$c(\boldsymbol{\xi}) = \frac{\theta}{2\pi}, \tag{24}$$

where θ is the internal angle of the corner in radians. If the internal angle subtended by the normals (γ) at corner is specified, the above equation can be rewritten as follows:

$$c(\boldsymbol{\xi}) = \frac{1}{2}\left(1 - \frac{\gamma}{\pi}\right). \tag{25}$$

4 NUMERICAL IMPLEMENTATION

For solving eq. (22) and obtaining the field variables, time axis and geometric boundary of the body must be discretized. In this equation, no approximation is involved until before of discretization and it is an exact relationship. As will be shown, to carry out the temporal integration the analytical process is elaborated and the numerical procedure is performed to spatial integration.

4.1 Temporal integration using linear time variation

For temporal integration, the interval from 0 to t was divided into N equal increments of duration Δt, that is, $t = N\Delta t$. Within each time step, the field variables could be assumed to remain linearly. Hence, the field variables are:

$$f(\boldsymbol{x}, \tau) = \sum_{n=1}^{N} \phi_1(\tau) f^n(\boldsymbol{x}) + \phi_2(\tau) f^{n-1}(\boldsymbol{x}), \tag{26}$$

where $f(\boldsymbol{x}, \tau)$ stands for displacement $u(\boldsymbol{x}, \tau)$ or traction $q(\boldsymbol{x}, \tau)$, $\phi_1(\tau)$ and $\phi_2(\tau)$ are the temporal interpolation functions corresponding to the forward and backward time nodes during a time step, respectively, as follows:

$$\phi_1(\tau) = \frac{\tau - (n-1)\Delta t}{\Delta t} M_n(\tau); \quad \phi_2(\tau) = \frac{n\Delta t - \tau}{\Delta t} M_n(\tau), \qquad (n-1)\Delta t \le \tau \le n\Delta t,$$

$$M_n(\tau) = H[\tau - (n-1)\Delta t] - H[\tau - n\Delta t]. \tag{27}$$

However, time-convoluted integrals of eq. (22) can be denoted by:

$$U_i^{N-n+1}(\boldsymbol{x}, \boldsymbol{\xi}) = \int_{(n-1)\Delta t}^{n\Delta t} u^*(\boldsymbol{x}, N\Delta t; \boldsymbol{\xi}, \tau) \phi_i(\tau) \mathrm{d}\tau; \quad i = \overline{1, 2}, \tag{28}$$

and

$$Q_i^{N-n+1}(\boldsymbol{x}, \boldsymbol{\xi}) = \int_{(n-1)\Delta t}^{n\Delta t} q^*(\boldsymbol{x}, N\Delta t; \boldsymbol{\xi}, \tau) \phi_i(\tau) \mathrm{d}\tau; \quad i = \overline{1, 2}. \tag{29}$$

After temporal integrations, the time-convoluted BIE took the following form:

$$c(\boldsymbol{\xi}) u^N(\boldsymbol{\xi}) = \sum_{n=1}^{N} \int_\Gamma \left(\begin{array}{l} \left[U_1^{N-n+1}(\boldsymbol{x}, \boldsymbol{\xi}) q^n(\boldsymbol{x}) + U_2^{N-n+1}(\boldsymbol{x}, \boldsymbol{\xi}) q^{n-1}(\boldsymbol{x}) \right] - \\ \left[Q_1^{N-n+1}(\boldsymbol{x}, \boldsymbol{\xi}) u^n(\boldsymbol{x}) + Q_2^{N-n+1}(\boldsymbol{x}, \boldsymbol{\xi}) u^{n-1}(\boldsymbol{x}) \right] \end{array} \right) \mathrm{d}\Gamma(\boldsymbol{x}) + u^{ff.N}(\boldsymbol{\xi}), \tag{30}$$

where U_1^{N-n+1} and U_2^{N-n+1} are the half-plane displacement time-convoluted kernels, Q_1^{N-n+1} and Q_2^{N-n+1} are the half-plane traction time-convoluted kernels corresponding to the forward and backward time nodes within a time step, respectively, and u^N and $u^{ff.N}$ stand for

the boundary displacement and the free field displacement at time $t = N\Delta t$, respectively. The full-plane displacement and traction time-convoluted kernels for antiplane elastodynamics can be found in Israil & Banerjee (1990a), Israil *et al.* (1992) and Banerjee (1994). On the time axis with the linear variation, the backward time node of the current time step is always covered by the forward time node of the previous time step. Hence, after simplifying and eliminating singularity terms in wave fronts, eq. (30) can be rewritten as follows:

$$c(\boldsymbol{\xi})\,u^N(\boldsymbol{\xi}) = \sum_{n=1}^{N}\int_{\Gamma}\begin{pmatrix}\left[U_1^{N-n+1}(\boldsymbol{x},\boldsymbol{\xi}) + U_2^{N-n}(\boldsymbol{x},\boldsymbol{\xi})\right]q^n(\boldsymbol{x}) - \\ \left[Q_1^{N-n+1}(\boldsymbol{x},\boldsymbol{\xi}) + Q_2^{N-n}(\boldsymbol{x},\boldsymbol{\xi})\right]u^n(\boldsymbol{x})\end{pmatrix}\mathrm{d}\Gamma(\boldsymbol{x}) + u^{ff.N}(\boldsymbol{\xi}), \tag{31}$$

where $U_1^{N-n+1} + U_2^{N-n}$ and $Q_1^{N-n+1} + Q_2^{N-n}$ are the condensed closed-form of half-plane displacement and traction time-convoluted kernels, respectively, which are given in Appendix (see eqs A1 and A2). In this form of BIE, the spatial numerical integration can be applied straightforward.

4.2 Spatial integration

To accomplish the spatial integration, which is carried out numerically, the boundary of the domain is discretized with isoparametric quadratic elements. Subsequently, all the quantities such as geometry and field variables are given in terms of the nodal variables as:

$$x_i(\kappa) = N_\alpha(\kappa)\,x_{i\alpha},$$

$$f(\boldsymbol{x}(\kappa)) = N_\alpha(\kappa)\,f_\alpha, \tag{32}$$

where f stands for the displacement and traction, $i = 1, 2$, $\alpha = 1, 2, 3$; $N_\alpha(\kappa)$ are quadratic shape functions and κ is the local intrinsic coordinates of the elements. With the spatial discretization, eq. (31) has in the following form:

$$c(\boldsymbol{\xi})\,u^N(\boldsymbol{\xi}) = \sum_{n=1}^{N}\sum_{m=1}^{M}\begin{bmatrix}\displaystyle\int_{\Gamma_m}\left[U_1^{N-n+1}(\boldsymbol{x}(\kappa),\boldsymbol{\xi}) + U_2^{N-n}(\boldsymbol{x}(\kappa),\boldsymbol{\xi})\right]N_\alpha(\kappa)\,|J|\,\mathrm{d}\kappa\,q_\alpha^n - \\ \displaystyle\int_{\Gamma_m}\left[Q_1^{N-n+1}(\boldsymbol{x}(\kappa),\boldsymbol{\xi}) + Q_2^{N-n}(\boldsymbol{x}(\kappa),\boldsymbol{\xi})\right]N_\alpha(\kappa)\,|J|\,\mathrm{d}\kappa\,u_\alpha^n\end{bmatrix} + u^{ff.N}(\boldsymbol{\xi}), \tag{33}$$

where M represents the total number of BEs, Γ_m stands for portion of the boundary to which element 'm' belongs and J is the Jacobian of transformation that could be obtained from the following equation:

$$J_i = \frac{\partial N_\alpha(\kappa)}{\partial\kappa}x_{i\alpha}. \tag{34}$$

4.3 Evaluation of singular part integration

At the first time step (i.e. for $N = n$), when the collocation point (source) is in the integration element, evaluation of special conditions is necessary for spatial integration of eq. (33). In this case, for eq. (A2), as the denominator (i.e. r or r') goes to zero, the numerator (i.e. $\partial r/\partial n$ or $\partial r'/\partial n$) goes to zero as well. Hence, traction time-convoluted kernel has a removable singularity on the order of $O(1)$ and regular Gauss quadrature is performed easily to integrate. However, on the other hand, displacement time-convoluted kernel has a singularity $O(\ln 1/rr')$ that requires taking special schemes. In this regard, eq. (A1) can be separated into singular and non-singular parts as follows:

$$\text{Eq. (A1)} = \{\text{Non-singular part}\} + \frac{1}{2\pi}\ln\left(\frac{1}{rr'}\right), \tag{35}$$

where only the second term is singular and it has the same singularity as the static fundamental solutions (Brebbia & Dominguez 1989; Dominguez 1993). For non-singular part, the regular Gauss quadrature is used and a special logarithmic numerical quadrature is applied to carry out the integration of singular part. It should be noted that, in spite of the established models on full-plane time-domain BEM, to promote the singularity problems in this study, no indirect method was used as the concept of rigid body motion and region of interest was a non-closed boundary. In this case, it was not required to define the fictitious elements, known as 'enclosing elements'.

4.4 Time stepping algorithm

After spatial integration of eq. (33) for each boundary node, it can be written in the following matrix form:

$$\sum_{n=1}^{N}\boldsymbol{H}^{N-n+1}\{\boldsymbol{u}^n\} = \sum_{n=1}^{N}\boldsymbol{G}^{N-n+1}\{\boldsymbol{q}^n\} + \{\boldsymbol{u}^{ff.N}\}, \tag{36}$$

where $\boldsymbol{H}^{N-n+1}$ and $\boldsymbol{G}^{N-n+1}$ are the matrices whose elements are obtained by integration over the BEs, $\{\boldsymbol{u}^n\}$ and $\{\boldsymbol{q}^n\}$ are vectors of boundary nodal quantities at the time step n. By applying the boundary conditions to the nodes and setting the unknown on the left, the above equation can be reordered as:

$$[\boldsymbol{A}_1^1]\{\boldsymbol{X}^N\} = [\boldsymbol{B}_1^1]\{\boldsymbol{Y}^N\} + \{\boldsymbol{R}^N\} + \{\boldsymbol{u}^{ff.N}\}, \tag{37}$$

where $\{\boldsymbol{X}^N\}$ and $\{\boldsymbol{Y}^N\}$ are the vectors of the unknown and known variables, respectively, and $\{\boldsymbol{R}^N\}$ involves the effects of past dynamic history on the current time node N, as:

$$\{\boldsymbol{R}^N\} = \sum_{n=1}^{N-1} \left(\boldsymbol{G}^{N-n+1}\{\boldsymbol{q}^n\} - \boldsymbol{H}^{N-n+1}\{\boldsymbol{u}^n\}\right). \tag{38}$$

Solving eq. (37) gives all boundary unknowns at each time step. Once eq. (37) is solved, it is possible to obtain displacements at any internal point m in domain. Then:

$$\{\boldsymbol{u}^{N.m}\} = \sum_{n=1}^{N} \left(\boldsymbol{G}^{\langle N-n+1\rangle.m}\{\boldsymbol{q}^n\} - \boldsymbol{H}^{\langle N-n+1\rangle.m}\{\boldsymbol{u}^n\}\right) + \{\boldsymbol{u}^{ff.N.m}\}, \tag{39}$$

where $\boldsymbol{u}^{N.m}$ and $\boldsymbol{u}^{ff.N.m}$ are displacement and free field response at any arbitrary internal point, respectively, $\boldsymbol{G}^{N-n+1.m}$ and $\boldsymbol{H}^{N-n+1.m}$ are matrices whose elements depend on the location of internal points and boundary nodes.

5 VALIDATION EXAMPLES

The formulation described above was implemented in a general half-plane BEM code as DASBEM (Dynamic Analysis of Structures using Boundary Element Method). To demonstrate the applicability and accuracy of this algorithm (as case 1 was denoted in the following) for the analysis of engineering problems, three different examples are solved and their results were compared with other published works. In addition, a separate full-plane BEM code (as case 2) was prepared by Israil and Banerjee's full-plane formulation (Israil & Banerjee 1990a) and was applied for analysing the considered examples.

5.1 A half-plane under Heaviside-type forcing function

In the first example, a half-plane with a surface free from traction due to uniformly distributed loading with a time dependence of a Heaviside function type was considered. This example showed the applicability and efficiency of the presented formulation in problems involving external loads. Fig. 2 represents dimensionless displacement at three points A, B and C on the ground surface versus dimensionless time. All the parameters and quantities are denoted in the mentioned figure.

As shown in Fig. 3, to solve this example, two types of the model were prepared which were established by (i) the half-plane time-domain BEM (case 1) and (ii) the full-plane time-domain BEM (case 2). The first case had only 10 quadratic BEs or 21 nodes at the loading place. The second case was modeled by 10 BEs at the loading place and 114 BEs at beyond the loading or totally 249 nodes. Also, to apply the suddenly stress variation effects at the corners (Fig. 3a), the proposed double-node technique was used (Mansur 1983). The problem was solved using 40 time steps with $\Delta t = 0.05$. Compared with the analytical solution (as can be found in Wang & Takemia 1992), the accuracies of the results were favourable, especially for case 1.

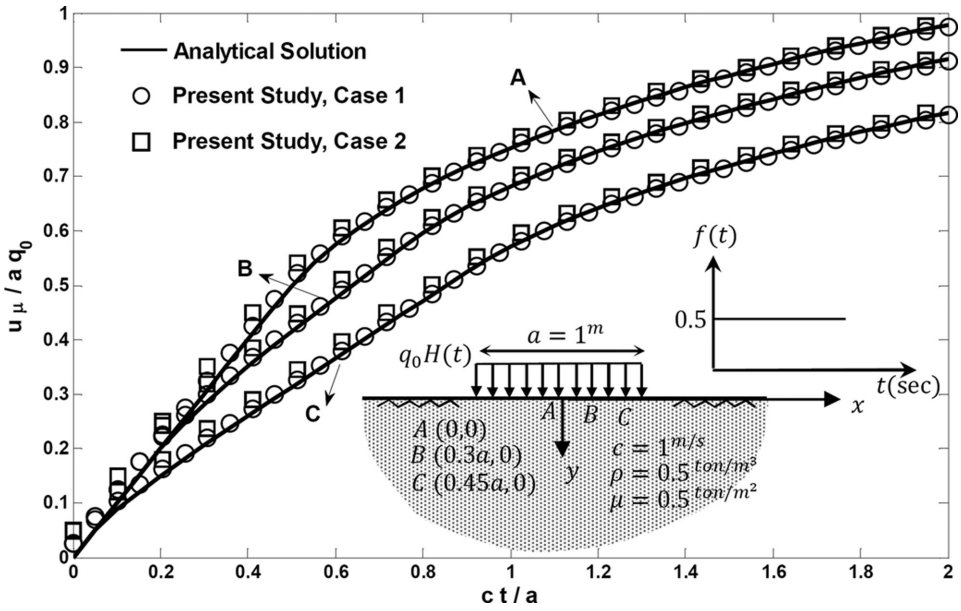

Figure 2. Comparison of analytical solution and boundary element models for an elastic half-plane due to uniformly distributed loading with a time dependence of a Heaviside function type; horizontal axis denotes the dimensionless time and vertical axis is dimensionless displacement with u as actual displacement.

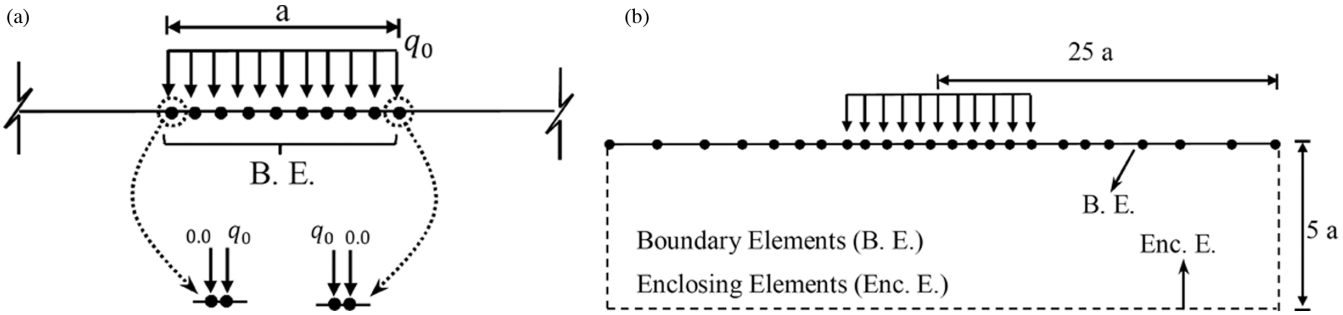

Figure 3. Schematic boundary element models for a linearly elastic half-plane subjected to uniform traction by: (a) the half-plane time-domain BEM (case 1); (b) the full-plane time-domain BEM (case 2).

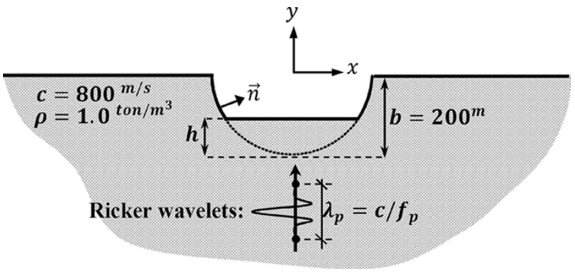

Figure 4. A definition sketch for a full/truncated semi-circular canyon under vertically propagating incident *SH* waves of Ricker type.

5.2 A full/truncated semi-circular canyon

In this example and the next one, application of the presented formulation and potency of the prepared algorithm were shown in analysing the seismic problems and obtaining the site response. At first, a full/truncated semi-circular canyon was considered due to vertically propagating incident *SH* waves (Fig. 4). Herein, incident motion was assumed as Ricker wavelets with λ_p representative wavelength (Ricker 1953):

$$f(t) = \left[1 - 2\left(\pi f_p (t - t_0)\right)^2\right] \mathrm{e}^{-\left(\pi f_p (t-t_0)\right)^2}, \tag{40}$$

where $f(t)$ denotes the function form of Ricker wavelet versus time history, f_p and t_0 are the predominant frequency and time-shift parameter, respectively. Taking into account eq. (40), the displacement of *SH* wave incidence for vertical propagation was represented as follows:

$$u^{\text{inc.}}(y, t) = a_{\max} \,.\, f\left(\alpha^{\text{inc.}}\right) H\left(t - \frac{|y|}{c}\right), \tag{41}$$

in which $a_{\max}$ and $H(.)$ indicate the maximum displacement time history and Heaviside function, respectively, and argument $\alpha^{\text{inc.}}$ denotes the phase of incident waves at location $|y|$ and time t to be measured from a specified location in which the ground surface is considered. To satisfy the stress-free conditions on the ground surface, a reflected wave with a reverse phase must be assumed:

$$u^{\text{ref.}}(y, t) = a_{\max} \,.\, f\left(\alpha^{\text{ref.}}\right) H\left(t - \frac{|y|}{c}\right), \tag{42}$$

where $\alpha^{\text{ref.}}$ indicates the phase of reflected waves. Hence, input motion (free field displacement) would be:

$$u^{ff}(y, t) = a_{\max} \,.\, \left(\begin{array}{l} \left[1 - 2\left(\frac{\pi f_p}{c}\alpha^{\text{inc.}}\right)^2\right] \mathrm{e}^{-\left(\frac{\pi f_p}{c}\alpha^{\text{inc.}}\right)^2} + \\ \left[1 - 2\left(\frac{\pi f_p}{c}\alpha^{\text{ref.}}\right)^2\right] \mathrm{e}^{-\left(\frac{\pi f_p}{c}\alpha^{\text{ref.}}\right)^2} \end{array} \right) H\left(t - \frac{|y|}{c}\right). \tag{43}$$

So,

$$\alpha^{\text{inc.}} = c\,(t - t_0) + |y|\,; \quad \alpha^{\text{ref.}} = c\,(t - t_0) - |y|\,. \tag{44}$$

It should be noted that, while using full-plane BEM, $\alpha^{\text{ref.}}$ was equal to zero.

One of the important factors in stability evaluations of time-domain BEM analysis is proper selection for time step and nodes interval. This can be expressed by defining the dimensionless parameter β as:

$$\beta = \frac{c\Delta t}{\Delta l}, \tag{45}$$

where c, Δt and Δl are shear wave velocity, time step and distance between nodes, respectively. In fact, parameter β indicates the number of elements in a time step when the seismic wave passes. In the use of time steps, it is recommended that β be close to 1 for elastodynamics problems with uniform meshes (Dominguez & Gallego 1991). Thus, the effect of parameter β is investigated for this example with the

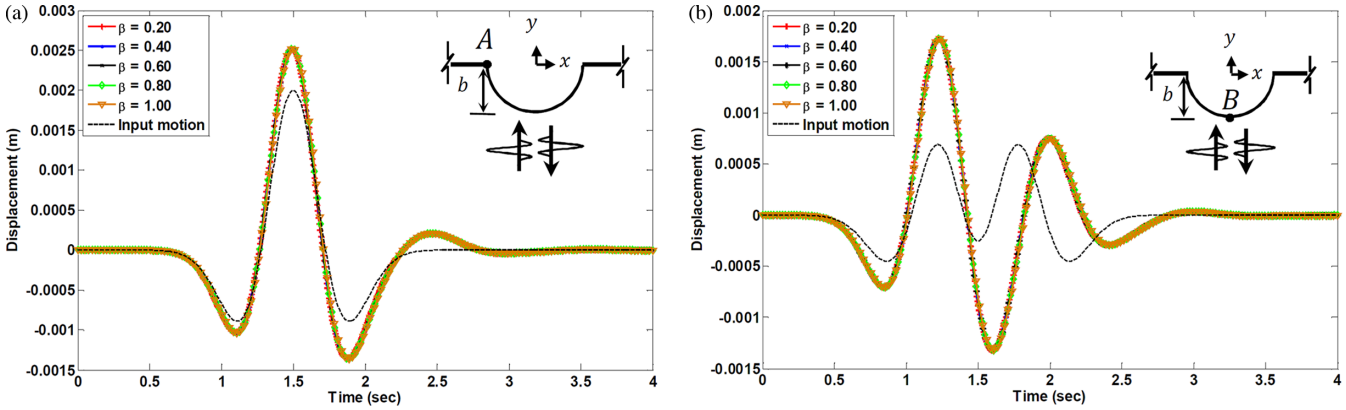

Figure 5. Time-domain displacement on the surface of semi-circular canyon for different values of β in: (a) edge of the canyon (point A); (b) the canyon floor (point B).

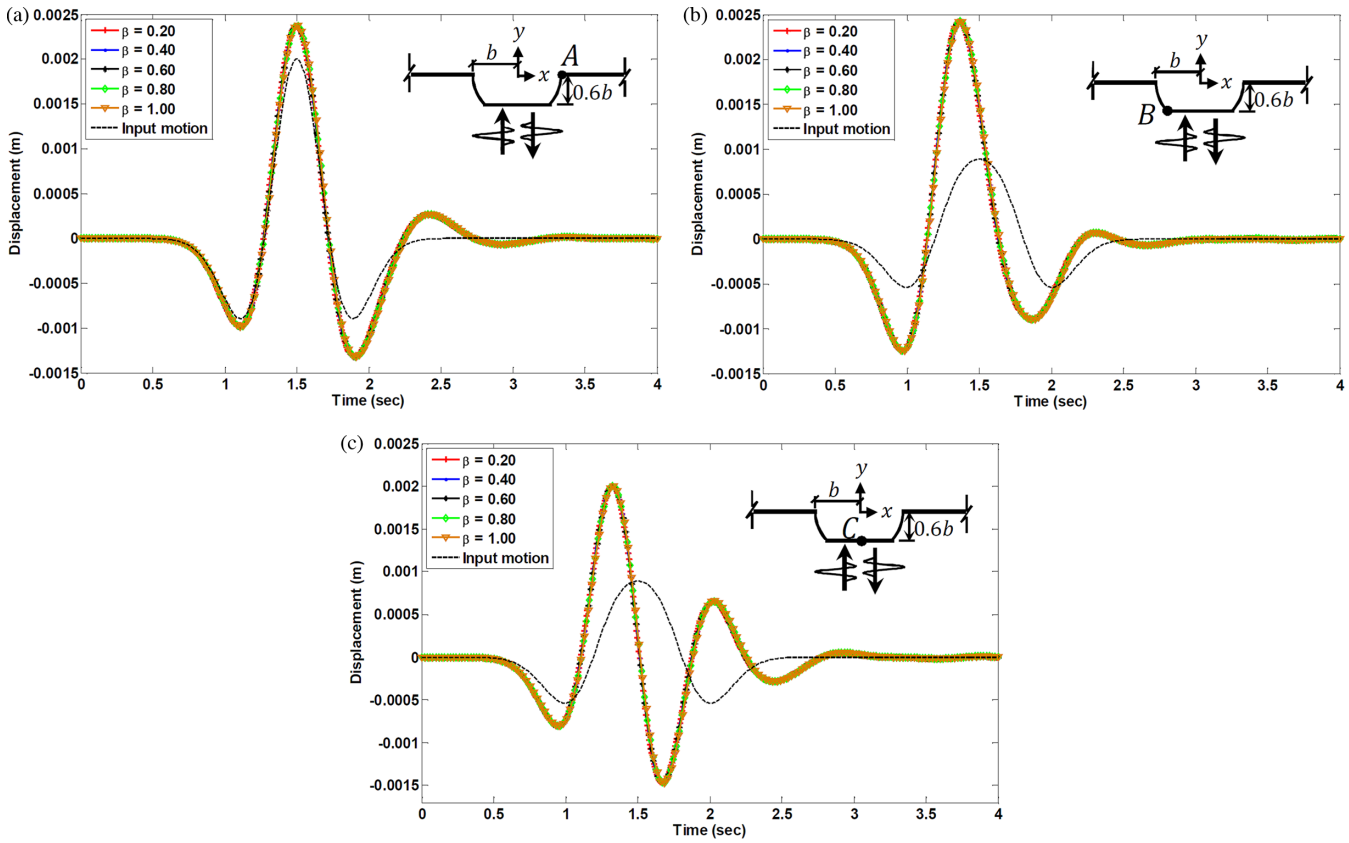

Figure 6. Time-domain displacement on the surface of truncated semi-circular canyon for different values of β in the: (a) upper edge (point A); (b) edge of the flat surface (point B); (c) middle of the flat surface (point C).

assumed data in Fig. 4. The dimensionless truncation thickness (h/b) was selected as 0.4 in this section. Distance of nodes was equal to 20 m (i.e. considering 31 and 27 nodes, only on the surface of the full and truncated canyons, respectively) and shear wave velocity was equal to 800 m s^{-1}; thus, the values of time steps changed from 0.005 to 0.025. This change caused β to be 0.2 to 1, respectively. The predominant frequency, time-shift parameter and maximum amplitude of *SH* wave of Ricker type were equal to 2 Hz, 1.5 s and 0.001 m, respectively. In Figs 5 and 6, the time-domain ground response for different points of canyon surface is given. As can be seen, the responses were steady to the change of β parameter. Hence, to optimize the number of time steps and obtain the acceptable response, β was chosen as 1 in this example.

Similar to the previous example, to compare the half-plane and full-plane time-domain BEM in the seismic analysis of canyon structures, two types of models were produced as cases 1 and 2, respectively. Fig. 7 shows discretized zones for two models. Models' details are shown in Table 1. Ricker wavelet specifications were equal to 3.0 Hz, 1.0 s and 0.001 m, for predominant frequency, time-shift parameter and maximum amplitude, respectively. The problem was solved by 120 time steps with Δt equal to 0.025. It deserves mentioning that the same number of nodes was used to discretize the canyon surface in two models, as in Table 1.

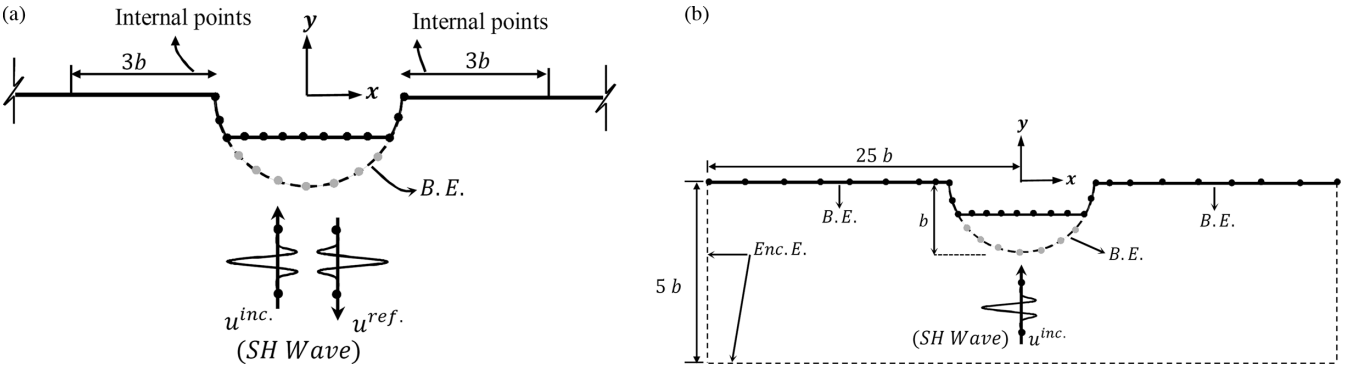

Figure 7. Schematic boundary element models for a full/truncated semi-circular canyon subjected to vertically propagating incident *SH* waves by: (a) the half-plane time-domain BEM (case 1); (b) the full-plane time-domain BEM (case 2).

Table 1. Models' specifications for a full/truncated semi-circular canyon.

	Models' details					
	case 1			case 2		
	N.D. (m)	N.N.	Int. P.	N.D.[a] (m)	N.N. (canyon)	N.N. (beyond the canyon)
Full	20	31	40	20	31	184
Truncated $h = 0.75b$	20	23	60	20	23	184
Truncated $h = 0.50b$	20	25	60	20	25	184
Truncated $h = 0.25b$	20	29	60	20	29	184

[a]The distance of nodes increases to 200 m at beyond the canyon for case 2.
N.D., nodes distance; N.N., number of nodes; Int. P., number of internal points.

To obtain the site response, further studies were done in the frequency domain. Generally, response amplitude of ground surface is presented at specific dimensionless frequencies in the frequency domain. Therefore, to compare the results of the current study with those of other published works, dimensionless frequency relationship must be defined as follows:

$$\eta = \frac{\omega b}{\pi c}, \tag{46}$$

where ω is the angular frequency of incident wave, b is the radius of canyon and c is the shear wave velocity. In Fig. 8, normalized displacement amplitude of semi-circular canyon surface and its beyond are plotted and compared with other published analytical and numerical solutions at dimensionless frequencies 0.25, 0.75, 1.25 and 2.0. Normalized displacement amplitude was defined as the ratio of the Fourier amplitude of the total motion obtained by BEM to the Fourier amplitude of the incident motion. The semi-circular canyon structures were solved by Trifunac (1972), Kawase (1988) and Reinoso *et al.* (1993) using transformed-domain methods. In addition, this problem was solved by Hirai (1988) using Mansur's BEM formulation (Mansur 1983) in the time domain. As can be shown, in spite of the insignificant difference at low dimensionless frequencies (i.e. 0.25 and 0.75), good agreement was observed between the current study and other published solutions. Cases 1 and 2 were quite consistent for semi-circular canyon.

Fig. 9 compares normalized displacement amplitude with respect to normalized x-direction for a truncated semi-circular canyon between the current study and an analytical solution. Tsaur & Chang (2009) have studied this problem recently. In different dimensionless truncation thickness (h/b), the results were very good agreement at dimensionless frequency of 2.0. Similar to semi-circular canyon, accuracy of the responses was the same between case 1 and case 2.

5.3 An embedded full/truncated circular cavity

In this example, displacement response of an elastic half-plane containing an unlined full/truncated circular cavity subjected to vertically propagating incident *SH* waves was obtained by the presented formulation and was compared with other existing solutions. Schematic geometry of the problem is shown in Fig. 10. To obtain acceptable responses for this problem, the distance between nodes was considered equal to 10 m. Depending on the depth of the cavity (H), the number of time steps and time-shift parameter (t_0) had different values. In spite of the canyon structures, in which the distance between wave front to ground surface was not far, in the embedded cavity problems, much time was necessary to take the forward waves to the ground surface and reflect them. The closest node to wave front (i.e. bottom node of cavity wall) in vertically propagating waves obtained the value of t_0 and the farthest node from the wave front (i.e. ground surface nodes) determined the number of time steps. The number of time steps, value of t_0 and details of models could be seen in Table 2. The predominant frequency and maximum amplitude of Ricker wavelet type were the same as those of the previous example.

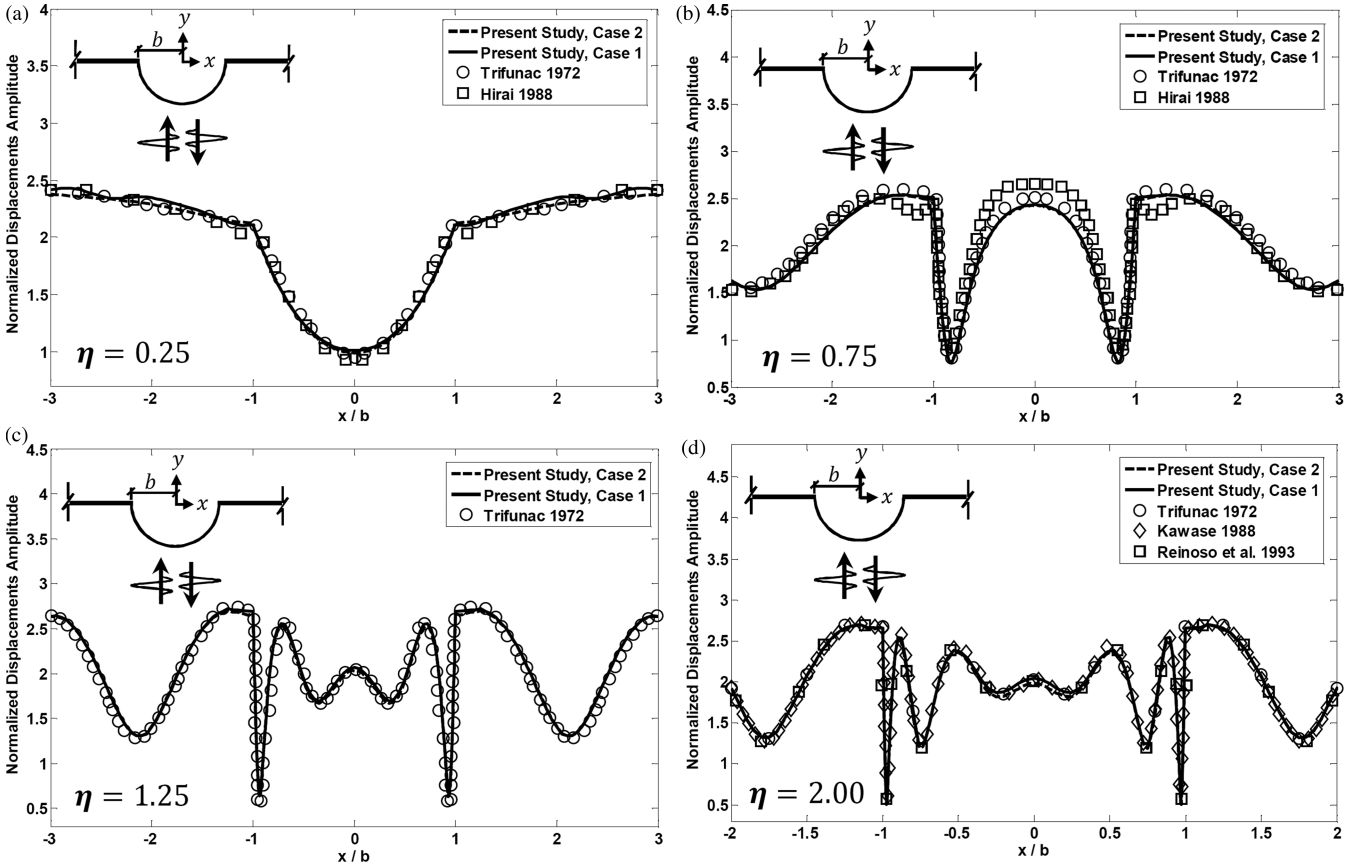

Figure 8. Normalized displacement amplitude on the surface of semi-circular canyon versus x/b at: (a) $\eta = 0.25$; (b) $\eta = 0.75$; (c) $\eta = 1.25$; (d) $\eta = 2$.

Fig. 11 shows the normalized displacement amplitude of ground surface involving a circular cavity embedded in the depth of 1.5b for dimensionless frequencies 0.5, 1.0, 1.5 and 2.0. The published solutions of this problem were presented by Lee (1977), Benites *et al.* (1992) and Luco & deBarros (1994) in the frequency domain. Lee (1977) demonstrated an analytical solution and two other solutions were carried out by indirect BEM. Compared with the mentioned solutions, the present studies were in good agreement. However, the remarkable thing was that disagreement could be observed between cases 1 and 2 at the top of the cavity on the ground surface ($-b < x < b$) at the dimensionless frequency of 2.0. As can be seen, case 1 represented better accuracy.

Fig. 12 shows ground response in the presence of an embedded cavity in the depth of 5b. Accuracy of the results was favourable. As can be seen, with increasing the cavity depth, at all dimensionless frequencies, disagreement could be observed between cases 1 and 2. Similar to depth 1.5b, compared with other solutions, accuracy of case 1 was always better that of than case 2. It deserves mentioning that cases 1 and 2 are modelled in the same conditions.

It should be mentioned that not only the results of this study (case 1), but also the results of Benites *et al.* (1992) as well as the results of Luco & deBarros (1994), differ slightly in few points with the results of Lee (1977). In other words, wherever the results of this study (case 1) differ slightly with the results of Lee (1977), exactly the same difference can be seen between the results of Benites *et al.* (1992) as well as the results of Luco & deBarros (1994) with the results of Lee (1977). The authors guess that an important source of this small disagreement between the numerical and analytical results could be some probable simplifying assumptions that Lee (1977) maybe adopted in order to enable the problem to be solved analytically.

In Fig. 13, displacement amplitude of cavity wall is shown in the depth of 1.5b and 5b for dimensionless frequencies of 0.5 and 1.0. The agreement was good between case 1, case 2 and Luco and deBarros's solution.

Among the recent studies carried out on the effects of underground cavities and inclusions on the ground surface response, the results of Yu & Dravinski (2009) can be referred to. These researchers studied the effect of an embedded cavity in the depth of 2b at dimensionless frequency of 2.0 using frequency-domain direct BEM and used a full-plane fundamental solution for BEM formulation. As can be shown in Fig. 14, precision of the responses was excellent for a large range of ground surface ($-10b < x < 10b$), especially for case 1.

Fig. 15 shows response amplitude of a half-plane containing a truncated circular cavity immersed in different depths for dimensionless frequencies of 1.0 and 4.0. An analytical solution was presented by Tsaur & Chang (2012) for this problem. To illustrate the results, the dimensionless truncation thickness (h/b) was chosen as 0.4 by Tsaur & Chang (2012). As can be observed, even at high frequency ($\eta = 4.0$ or actual frequency of 8.0 Hz), the displacement responses were in very good agreement for case 1.

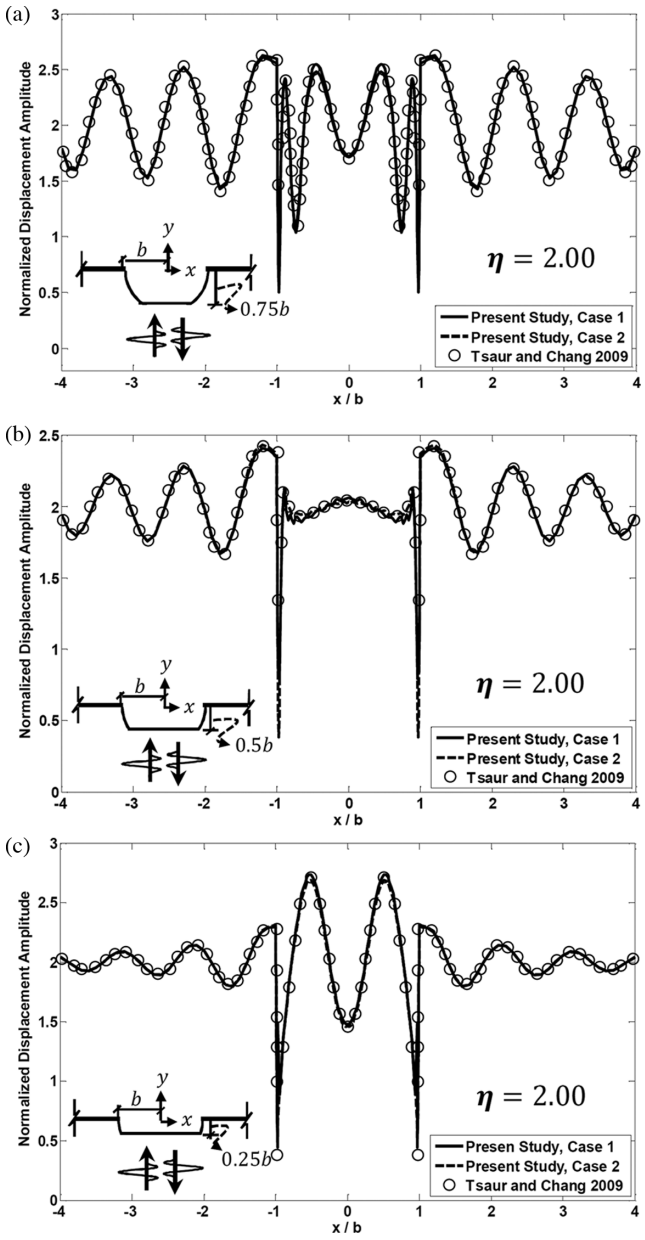

Figure 9. Normalized displacement amplitude on the surface of truncated semi-circular canyon versus x/b at dimensionless frequency of 2.0 for h/b equal to: (a) 0.25; (b) 0.5; (c) 0.75.

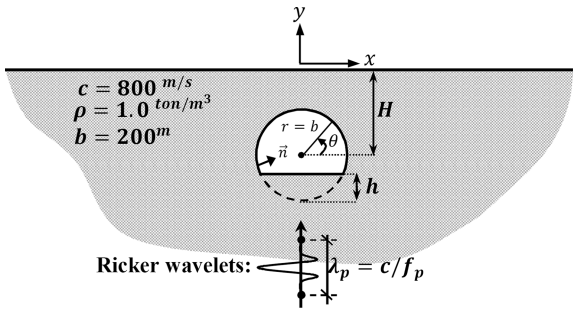

Figure 10. A definition sketch for an embedded full/truncated circular cavity under vertically propagating incident *SH* waves of Ricker type.

Table 2. Models' specifications for an embedded full/truncated circular cavity ($h/b = 0.4$).

		Models' details						
		case 1		case 2		case 1/case 2		
		N.N.	Int. P.	N.N. (the cavity)	N.N. (the ground surface)	$N^{\text{step}a}$	t_0 (s)	N.D. (m)
Full	$H = 1.5b$	126	121	126	225	150	1.60	10
	$H = 2.0b$	62	201	62	205	180	1.90	20
	$H = 5.0b$	126	121	126	225	280	3.30	10
Truncated	$H = 3.0b$	60	81	60	205	180	2.10	20
	$H = 5.0b$	60	81	60	205	270	3.10	20
	$H = 7.0b$	60	81	60	205	320	4.10	20

[a] N^{step} indicates the number of time steps.

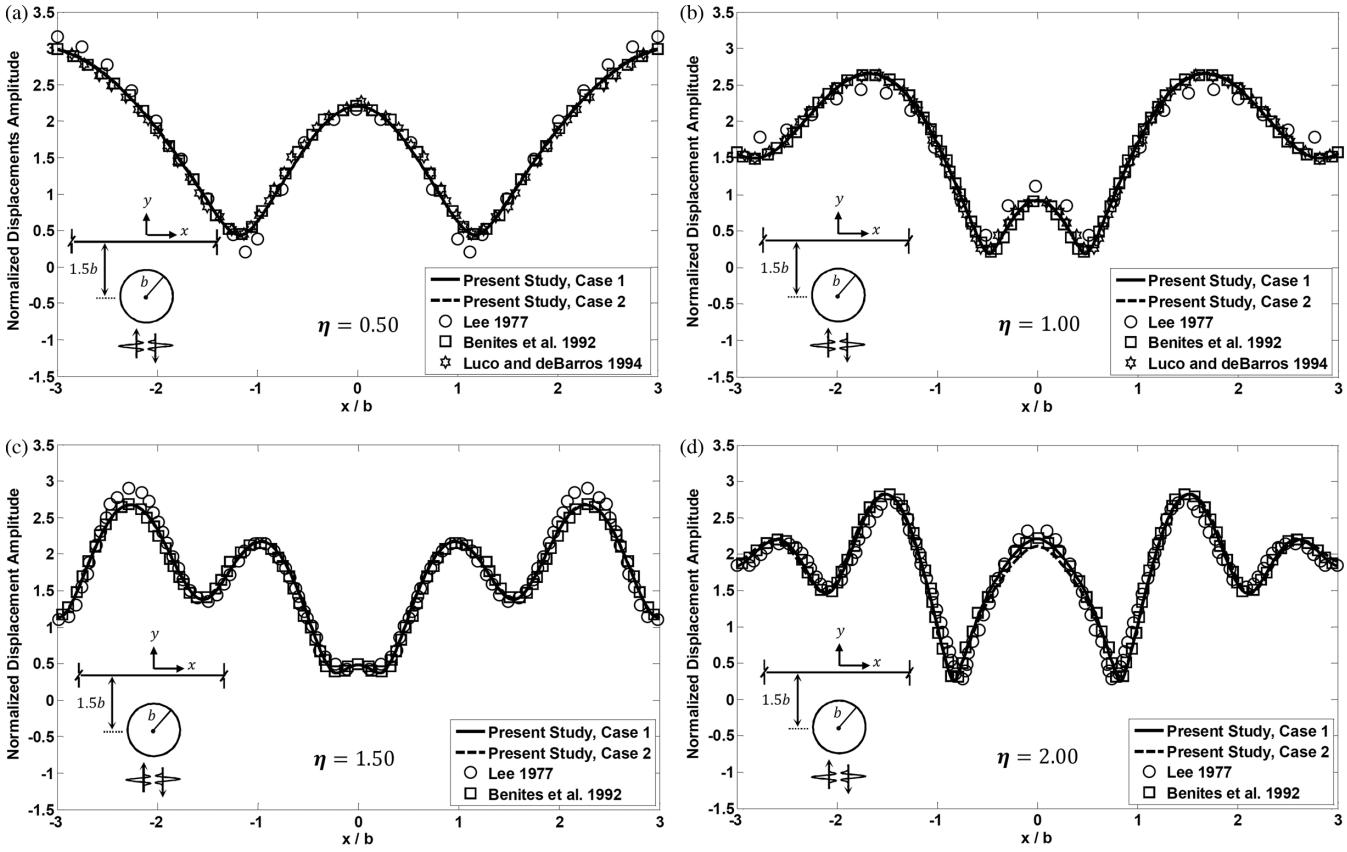

Figure 11. Normalized displacement amplitude on the ground surface versus x/b in the presence of an embedded cavity in depth of $1.5b$ at: (a) $\eta = 0.50$; (b) $\eta = 1.0$; (c) $\eta = 1.50$; (d) $\eta = 2.0$.

5.4 Analysis time

All the algorithms used in this study were written by MATLAB software. CPU time of all the examples is given in Table 3 in terms of second. As can be observed, using the half-plane time-domain BEM (case 1), the analysis time was reduced considerably. To analyse the example of the embedded cavity in the depth of $2b$ (Fig. 14), time of 250 s was reported by Yu (2008) in the frequency domain using a computer with similar capabilities. Compared with the time of 342 s obtained in this study (Table 3), the analysis time of this problem in the time domain seemed to be very favourable.

6 CONCLUSIONS

A half-plane time-domain BEM was presented in the paper to analyse the 2-D scalar wave problems in a linearly elastic medium. Taking the existing transient full-plane fundamental solution and mathematical method of source image into account, a time-domain half-plane fundamental solution was obtained for displacement and traction fields at first. Next, the half-plane time-convoluted kernels or, in other words, key elements of the proposed approach were extracted analytically by applying the time-convolution integral on them. Once the

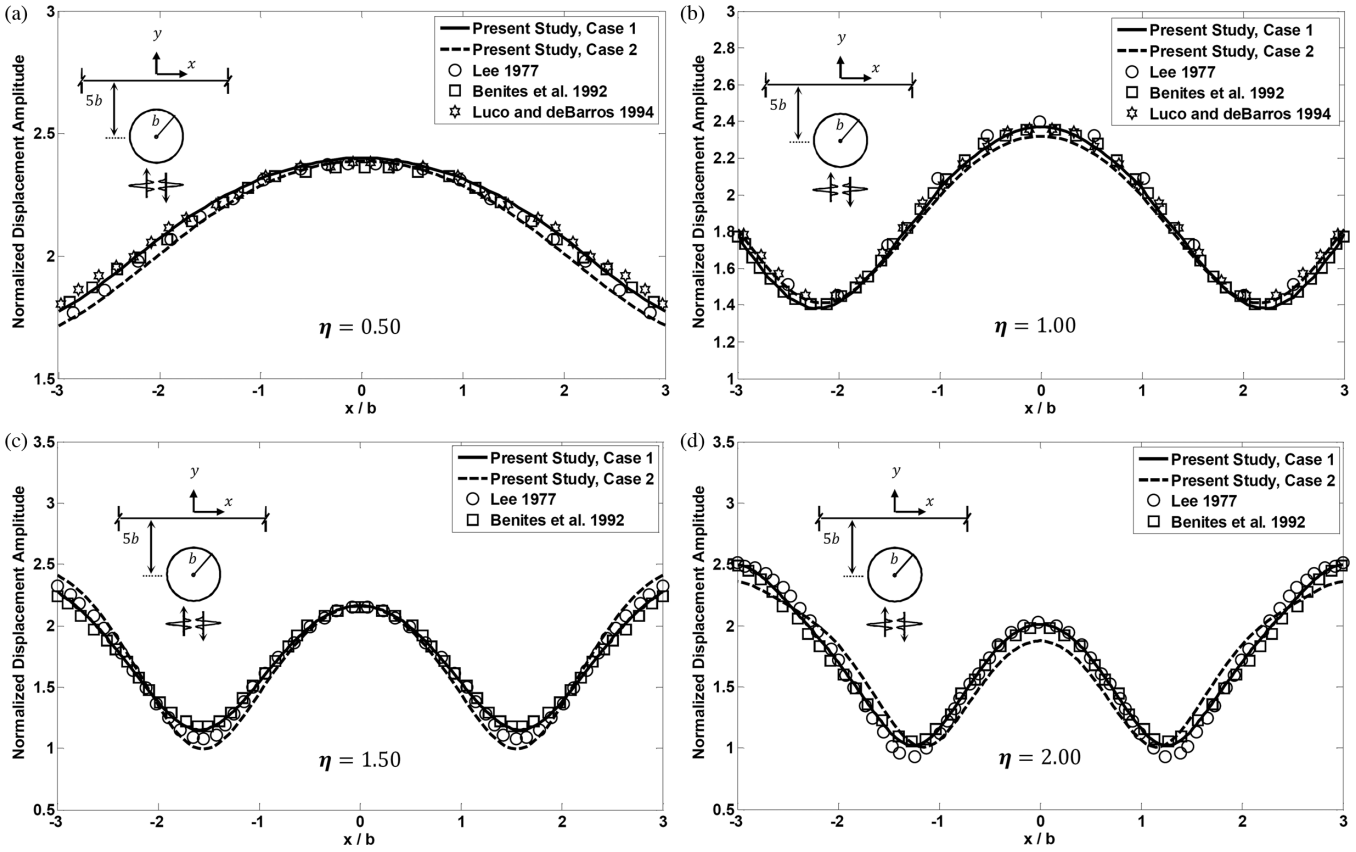

Figure 12. Normalized displacement amplitude on the ground surface versus x/b in the presence of an embedded cavity in depth of $5.0b$ at: (a) $\eta = 0.50$; (b) $\eta = 1.0$; (c) $\eta = 1.50$; (d) $\eta = 2.0$.

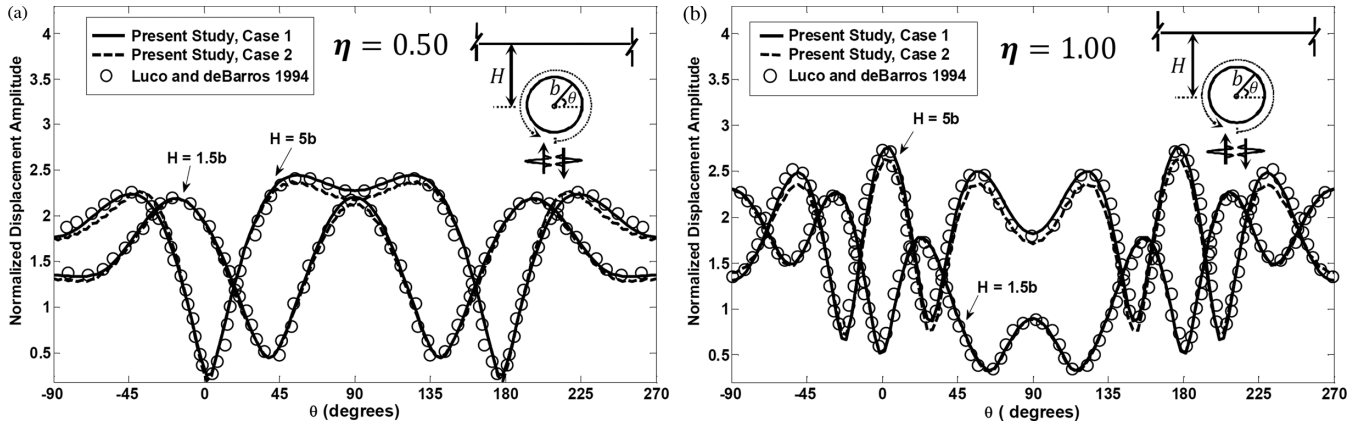

Figure 13. Normalized displacement amplitude on the cavity wall for H/b equal to 1.5 and 5.0 at: (a) $\eta = 0.50$; (b) $\eta = 1.0$.

half-plane time-domain BEM was implemented in computer codes, its applicability and efficiency were validated by the published solutions. In this regard, three different examples subjected to the external loads as well as seismic motions were examined. The studies showed that accuracy of the responses was in good agreement for all the examples and capability of the method was appropriately acceptable. In order to compare accuracy of the half-plane time-domain BEM (case 1) with the corresponding full-plane case (case 2) in completely the same conditions, a separate BEM code was accordingly prepared based on the full-plane time-domain BEM and it was seen that not only the results of the half-plane time-domain BEM had more capability and better accuracy, but also the analysis time was dramatically reduced. Whereas the half-plane time-domain BEM and the full-plane time-domain BEM used the same element dimensions as well as the same time step, the results obtained by the half-plane time-domain BEM possess a better accuracy. In other words, in problems that could be solved by both these methods, the half-plane time-domain BEM had the capability to give more accurate results in a much shorter time compared to the full-plane time-domain BEM.

Whereas the examples presented in this paper showed some advantages of the half-plane time domain BEM over the full-plane time domain BEM, it is obvious that the former had also some important limitations in comparison with the latter one. Seismic analysis of hills,

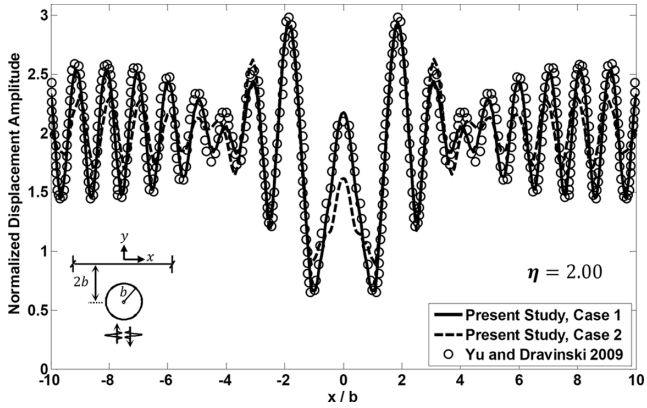

Figure 14. Normalized displacement amplitude on the ground surface versus x/b in the presence of an embedded cavity in the depth of $2.0b$ at dimensionless frequency of 2.0.

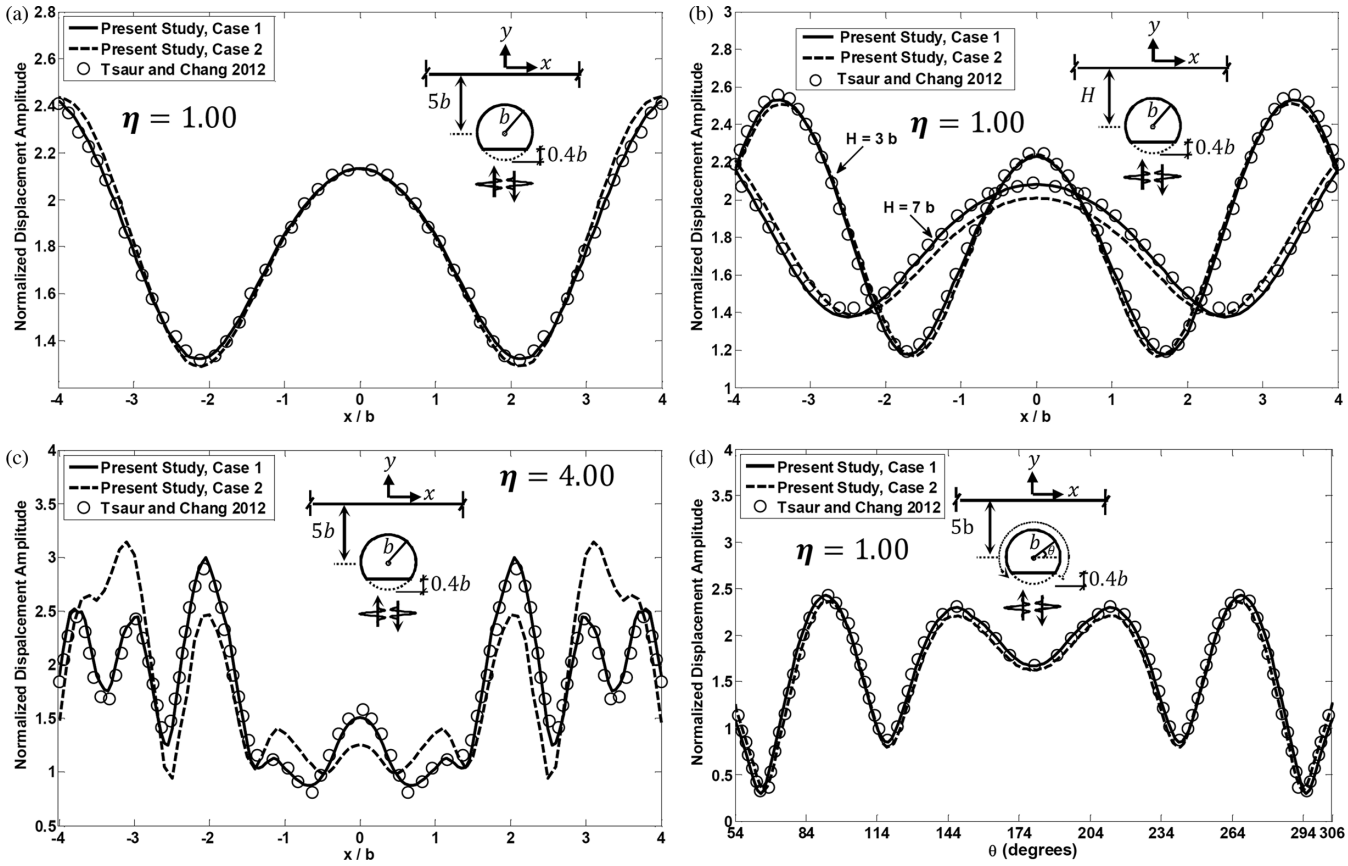

Figure 15. Normalized displacement amplitude of a half-plane containing embedded truncated circular cavity with $h/b = 0.40$: (a) ground surface response for $H/b = 5.0$ at $\eta = 1.0$; (b) ground surface response for H/b equal to 3.0 and 7.0 at $\eta = 1.0$; (c) ground surface response for $H/b = 5.0$ at $\eta = 4.0$; (d) response of cavity wall for $H/b = 5.0$ at $\eta = 1.0$.

ridges as well as non-homogenous mediums with the half-plane BEM was not so straightforward. Besides, due to the complexity of the half-space Green's function, they could not be simply extended to important cases such as anisotropic and viscoelastic media. This kind of problems could be solved more efficiently by the full-plane BEM. Combining the half-plane BEM with the full-space BEM and using the advantages of each method in its place seem to be another efficient way which should be experienced in the future.

ACKNOWLEDGEMENTS

The authors would like to express their gratitude to the respected editor, Prof. Xiaofei Chen, and two anonymous reviewers for their useful comments and precious time spent on our paper.

Table 3. The CPU times in terms of second from executing time-domain BEM codes with an Intel Core i7 CPU M640 at 2.8 GHz and 4 GB RAM.

			Case 1	Case 2
Example 1	A half-plane under uniform traction		3	99
	Full semi-circular canyon		38	564
Example 2	Truncated semi-circular canyon[a]	$h = 0.25b$	41	562
		$h = 0.50b$	35	538
		$h = 0.75b$	30	523
Example 3	Embedded full circular cavity[b]	$H = 1.50b$	654	3254
		$H = 2.00b$	342	2158
		$H = 5.00b$	1174	10 414
	Embedded truncated circular cavity	$H = 3.00b$	218	2042
		$H = 5.00b$	328	4673
		$H = 7.00b$	384	6424

[a]Analysis times are presented in different truncation thickness (h/b) for the canyon.
[b]Analysis times are presented in different dimensionless depths (H/b) for the embedded cavity.

REFRENCES

Ahmad, S. & Banerjee, P.K., 1988. Multi-domain BEM for two-dimensional problems of elastodynamics, *Int. J. Numer. Meth. Eng.,* **26**(4), 891–911.

Antes, H., 1985. A boundary elements procedure for transient wave propagation in two-dimensional isotropic elastic media, *Finite Elem. Anal. Des.,* **1**(4), 313–322.

Ausilio, E., Conte, E. & Dente, G., 2008. Seismic response of alluvial valleys to SH waves, *Seism. Eng. Conf., AIP Conf. Proc.,* **1020,** 199–206.

Banerjee, P.K., 1994. *Boundary Element Methods in Engineering,* McGraw-Hill Book Company, New York.

Belytschko, T. & Chang, H.S., 1988. Simplified direct time integration boundary element method, *J. Eng. Mech.,* **114**(1), 117–134.

Benites, R., Aki, K. & Yomogida, K., 1992. Multiple scattering of SH waves in 2-D media with many cavities, *Pure appl. Geophys.,* **138**(3), 353–390.

Beskos, D.E., 1987. Boundary element methods in dynamic analysis, *Appl. Mech. Rev.,* **40**(1), 1–23.

Beskos, D.E., 1997. Boundary element methods in dynamic analysis: part II (1986–1996), *Appl. Mech. Rev.,* **50**(3), 149–197.

Brebbia, C.A. & Dominguez, J., 1989. *Boundary Elements, an Introductory Course,* Computational Mechanics Publications, Southampton, Boston.

Cole, D.M., Kosloff, D.D. & Minster, J.B., 1978. A numerical boundary integral method for elastodynamics, *Bull. seism. Soc. Am.,* **68**(5), 1331–1357.

Cruse, T.A. & Rizzo, F.J., 1968. A direct formulation and numerical solution of the general transient elastodynamics problem I, *J. Math. Anal. Appl.,* **22**(1), 244–259.

De Hoop, A.T., 1960. A modification of Cagniard's method for solving seismic pulse problems, *Appl. Sci. Res., Sec. B,* **8**(1), 349–356.

Dominguez, J., 1993. *Boundary Elements in Dynamics,* Computational Mechanics Publications, Southampton, Boston.

Dominguez, J. & Gallego, R., 1991. The time domain boundary element method for elastodynamic problems, *Math. Comput. Modelling,* **15**(3–5), 119–129.

Dominguez, J. & Meise, T., 1991. On the use of the BEM for wave propagation in infinite domains, *Eng. Anal. Bound. Elem.,* **8**(3), 132–138.

Dravinski, M., 1982. Influence of interface depth upon strong ground motion, *Bull. seism. Soc. Am.,* **72**(2), 597–614.

Duffy, D.G., 2001. *Green's Functions with Applications,* Chapman & Hall/CRC Press, Boca Raton, FL.

Eringen, A.C. & Suhubi, E.S., 1975. *Elastodynamics,* Academic Press, New York.

Friedman, M.B. & Shaw, R., 1962. Diffraction of pulses by cylindrical obstacles of arbitrary cross section, *J. appl. Mech.,* **29**(1), 40–46.

Gallego, R. & Dominguez, J., 1990. A unified formulation of two existing time-domain boundary-element approaches, *Commun. Appl. Numer. Methods,* **6**(1), 17–25.

Haberman, R., 2004. *Applied Partial Differential Equations (with Fourier Series and Boundary Value Problems),* 4th edn, Prentice Hall, Englewood Cliffs, NJ.

Hadley, P.K., Askar, A. & Cakmak, A.S., 1989. Scattering of waves by inclusions in a nonhomogeneous elastic half space solved by boundary element methods, Technical Report NCEER-89–0027.

Hirai, H., 1988. Analysis of transient response of SH wave scattering in a half-space by the boundary element method, *Eng. Anal.,* **5**(4), 189–194.

Israil, A.S.M. & Banerjee, P.K., 1990a. Advanced development of time-domain BEM for two-dimensional scalar wave propagation, *Int. J. Numer. Methods Eng.,* **29**(5), 1003–1020.

Israil, A.S.M. & Banerjee, P.K., 1990b. Advanced time-domain formulation of BEM for two-dimensional transient elastodynamics, *Int. J. Numer. Methods Eng.,* **29**(7), 1421–1440.

Israil, A.S.M., Banerjee, P.K. & Wang, H.C., 1992. Time-domain formulations of BEM for two-dimensional, axisymmetric and three-dimensional scalar wave propagation, Chapter III, in *Advanced Dynamic Analysis by BEM,* pp. 75–114, eds Banerjee, P.K. & Kobayashi, S.K., Elsevier Applied Science, London.

Kamalian, M., Gatmiri, B. & Sohrabi-Bidar, A., 2003. On time-domain two-dimensional site response analysis of topographic structures by BEM, *J. Seism. Earthq. Eng.,* **5**(2), 35–45.

Kamalian, M., Jafari, M.K., Sohrabi-Bidar, A., Razmkhah, A. & Gatmiri, B., 2006. Time-domain two-dimensional site response analysis of non-homogeneous topographic structures by a hybrid FE/BE method, *Soil Dyn. Earthq. Eng.,* **26**(8), 753–765.

Kamalian, M., Gatmiri, B., Sohrabi-Bidar, A. & Khalaj, A., 2007. Amplification pattern of 2D semi-sine shaped valleys subjected to vertically propagating incident waves, *Commun. Numer. Methods Eng.,* **23**(10), 871–887.

Kamalian, M., Jafari, M.K., Sohrabi-Bidar, A. & Razmkhah, A., 2008a. Seismic response of 2D semi-sines shaped hills to vertically propagating incident waves: amplification patterns and engineering applications, *Earthq. Spectra,* **24**(2), 405–430.

Kamalian, M., Sohrabi-Bidar, A., Razmkhah, A., Taghavi, A. & Rahmani, I., 2008b. Considerations on seismic microzonation in areas with two-dimensional hills, *J. Earth Syst. Sci.,* **117**(2), 783–796.

Kawase, H., 1988. Time-domain response of a semi-circular canyon for incident SV, P, and Rayleigh waves calculated by the discrete wavenumber boundary element method, *Bull. seism. Soc. Am.,* **78**(4), 1415–1437.

Kontoni, D.N., Beskos, D.E. & Manolis, G.D., 1987. Uniform half-plane elastodynamic problems by an approximate boundary element method, *Soil Dyn. Earthq. Eng.,* **6**(4), 227–238.

Lee, V.W., 1977. On the deformations near circular underground cavity subjected to incident plane SH-waves, in *Proceedings of Symposium of Applications of Computer Methods in Engineering Conference,* University of Southern California, Los Angeles, pp. 951–962.

Luco, J.E. & deBarros, F.C.P., 1994. Dynamic displacements and stresses in the vicinity of a cylindrical cavity embedded in a half-space, *Earthq. Eng. Struct. Dyn.,* **23**(3), 321–340.

Manolis, G.D., 1983. A comparative study on three boundary element method approaches to problems in elastodynamics, *Int. J. Numer. Methods Eng.,* **19**(1), 73–91.

Manolis, G.D. & Beskos, D.E., 1981. Dynamic stress concentration studies by boundary integrals and Laplace transforms, *Int. J. Numer. Methods Eng.,* **17**(4), 573–599.

Mansur, W.J., 1983. A time-stepping technique to solve wave propagation problems using the boundary element method, *PhD dissertation,* University of Southampton.

Morse, P.M. & Feshbach, H., 1953. *Methods of Theoretical Physics,* McGraw-Hill Book Company, New York.

Niwa, Y., Fukui, T., Kato, S. & Fujiki, K., 1980. An application of the integral equation method to two-dimensional elastodynamics, *Theor. Appl. Mech.,* **28,** 281–290.

Ohtsu, M. & Uesugi, S., 1985. Analysis of SH wave scattering in a half space and its applications to seismic responses of geological structures, *Eng. Anal.,* **2**(4), 198–204.

Reinoso, E., Wrobel, L.C. & Power, H., 1993. Preliminary results of the modeling of the Mexico City valley with a two-dimensional boundary element method for the scattering of SH Waves, *Soil Dyn. Earthq. Eng.,* **12**(8), 457–468.

Rice, J.M. & Sadd, M.H., 1984. Propagation and scattering of SH-waves in semi-infinite domains using a time-dependent boundary element method, *J. Appl. Mech.,* **51,** 641–645.

Richter, C. & Schmid, G., 1999. A Green's function time-domain boundary element method for the elastodynamic half-plane, *Int. J. Numer. Methods Eng.,* **46**(5), 627–648.

Ricker, N., 1953. The form and laws of propagation of seismic wavelets, *Geophysics,* **18**(1), 10–40.

Sanchez-Sesma, F.J. & Campillo, M., 1991. Diffraction of P, SV, and Rayleigh waves by topographic features: a boundary integral formulation, *Bull. seism. Soc. Am.,* **81**(6), 2234–2253.

Sanchez-Sesma, F.J. & Campillo, M., 1993. Topographic effects for incident P, SV and Rayleigh waves, *Tectonophysics,* **218,** 113–125.

Sanchez-Sesma, F.J. & Esquivel, J.A., 1979. Ground motion on alluvial valleys under incident plane SH waves, *Bull. seism. Soc. Am.,* **69**(4), 1107–1120.

Soares, D., Jr. & Mansur, W.J., 2009. An efficient time-truncated boundary element formulation applied to the solution of the two-dimensional scalar wave equation, *Eng. Anal. Bound. Elem.,* **33**(1), 43–53.

Spyrakos, C.C. & Antes, H., 1986. Time domain boundary element method approaches in elastodynamics: a comparative study, *Comput. Struct.,* **24**(4), 529–535.

Spyrakos, C.C. & Beskos, D.E., 1986. Dynamic response of rigid strip-foundations by a time-domain boundary element method, *Int. J. Numer. Methods Eng.,* **23**(8), 1547–1565.

Trifunac, M.D., 1972. Scattering of plane SH waves by a semi-cylindrical canyon, *Earthq. Eng. Struct. Dyn.,* **1**(3), 267–281.

Tsaur, D. & Chang, K., 2009. Scattering of SH waves by truncated semicircular canyon, *J. Eng. Mech.,* **135**(8), 862–870.

Tsaur, D. & Chang, K., 2012. Multiple scattering of SH waves by an embedded truncated circular cavity, *J. Mar. Sci. Tech.,* **20**(1), 73–81.

Wang, C. & Takemia, H., 1992. Analytical elements of time domain BEM for two-dimensional scalar wave problems, *Int. J. Numer. Methods Eng.,* **33**(8), 1737–1754.

Wong, H.L. & Jennings, P.C., 1975. Effects of canyon topography on strong ground motion, *Bull. seism. Soc. Am.,* **65**(5), 1239–1257.

Yu, M.C., 2008. Scattering of a plane harmonic wave by a completely embedded corrugated scatterer, *PhD dissertation,* Faculty of the Graduate School, University of Southern California.

Yu, M.C. & Dravinski, M., 2009. Scattering of a plane harmonic SH wave by a completely embedded corrugated scatterer, *Int. J. Numer. Methods Eng.,* **78**(2), 196–214.

Yu, G., Mansur, W.J., Carrer, J.A.M. & Gong, L., 2000. Stability of Galerkin and collocation time domain boundary element methods as applied to the scalar wave equation, *Comput. Struct.,* **74**(4), 495–506.

APPENDIX: HALF-PLANE TIME-CONVOLUTED KERNELS

In eq. (31), the expressions of $U_1^{N-n+1}+U_2^{N-n}$ and $Q_1^{N-n+1}+Q_2^{N-n}$ were defined as:

$$U_1^{N-n+1}+U_2^{N-n}=\frac{1}{2\pi}\left[\begin{array}{l}\left(\begin{array}{l}(N-n+1)\cosh^{-1}\dfrac{(N-n+1)c\Delta t}{r}-\sqrt{(N-n+1)^2-\left(\frac{r}{c\Delta t}\right)^2}-\\ 2(N-n)\cosh^{-1}\dfrac{(N-n)c\Delta t}{r}+2\sqrt{(N-n)^2-\left(\frac{r}{c\Delta t}\right)^2}+\\ (N-n-1)\cosh^{-1}\dfrac{(N-n-1)c\Delta t}{r}-\sqrt{(N-n-1)^2-\left(\frac{r}{c\Delta t}\right)^2}\end{array}\right)+\\ \left(\begin{array}{l}(N-n+1)\cosh^{-1}\dfrac{(N-n+1)c\Delta t}{r'}-\sqrt{(N-n+1)^2-\left(\frac{r'}{c\Delta t}\right)^2}-\\ 2(N-n)\cosh^{-1}\dfrac{(N-n)c\Delta t}{r'}+2\sqrt{(N-n)^2-\left(\frac{r'}{c\Delta t}\right)^2}+\\ (N-n-1)\cosh^{-1}\dfrac{(N-n-1)c\Delta t}{r'}-\sqrt{(N-n-1)^2-\left(\frac{r'}{c\Delta t}\right)^2}\end{array}\right)\end{array}\right], \tag{A1}$$

$$Q_1^{N-n+1}+Q_2^{N-n}=-\frac{1}{2\pi}\left[\begin{array}{l}\left(\dfrac{1}{r}\dfrac{\partial r}{\partial n}\left\{\begin{array}{c}\sqrt{(N-n+1)^2-\left(\frac{r}{c\Delta t}\right)^2}-2\sqrt{(N-n)^2-\left(\frac{r}{c\Delta t}\right)^2}+\\ \sqrt{(N-n-1)^2-\left(\frac{r}{c\Delta t}\right)^2}\end{array}\right\}\right)+\\ \left(\dfrac{1}{r'}\dfrac{\partial r'}{\partial n}\left\{\begin{array}{c}\sqrt{(N-n+1)^2-\left(\frac{r'}{c\Delta t}\right)^2}-2\sqrt{(N-n)^2-\left(\frac{r'}{c\Delta t}\right)^2}+\\ \sqrt{(N-n-1)^2-\left(\frac{r'}{c\Delta t}\right)^2}\end{array}\right\}\right)\end{array}\right]. \tag{A2}$$